Available online at www.sciencedirect.com

jmr&t Journal of Materials Research and Technology

journal homepage: www.elsevier.com/locate/jmrt

Feasibility study on ultraprecision micro-milling of the additively manufactured NiTi alloy for generating microstructure arrays

Hanheng Du [a], *Chenliang Wu* [b], *Denghui Li* [a], *Wai Sze Yip* [a,d], *Zuankai Wang* [c], *Suet To* [a,d,*]

[a] *State Key Laboratory of Ultra-precision Machining Technology, Department of Industrial and Systems Engineering, The Hong Kong Polytechnic University, Hong Kong, China*

[b] *School of Materials Science and Engineering, Shenyang University of Technology, China*

[c] *Department of Mechanical Engineering, The Hong Kong Polytechnic University, Hong Kong, China*

[d] *The Hong Kong Polytechnic University Shenzhen Research Institute, Shenzhen, China*

ARTICLE INFO

Article history:
Received 17 April 2023
Accepted 23 May 2023
Available online 26 May 2023

Keywords:
Additive manufacturing
NiTi alloy
Ultraprecision micro-milling
Microstructure array
Surface wettability

ABSTRACT

Nickel-titanium (NiTi) alloy has unique functional properties in medical and microelectronics products. Recently, additive manufacturing has become an attractive way of fabricating NiTi alloy. However, the study of generating microstructure arrays on additively manufactured (AMed) NiTi alloy surfaces remains unclear. Motivated by this, this study proposes the ultraprecision micro-milling (UMM) process to generate microstructure arrays and perform a systematic investigation. First, selective laser melting, as a popular additive manufacturing way, was utilized to fabricate the AMed NiTi alloy. Then, the UMM process was carried out to machine these samples. After the machining experiments, a mirror surface with a surface roughness of 0.014 μm can be acquired, which demonstrates the good machinability of the AMed NiTi alloy. Moreover, the micro-groove array and micro-pillar array with low machining errors were machined on the AMed NiTi alloy surfaces, which verifies the effectiveness of the proposed machining process. The corresponding cutting forces, tool conditions, and chip morphologies were studied to fully understand the machining mechanism of the AMed NiTi alloy. Besides, the surface wettability of microstructure arrays was also quantitatively analyzed. Therefore, this study provides a facile and effective machining process for generating microstructure arrays on the AMed NiTi alloy surfaces.

1. Introduction

Nickel-titanium (NiTi) alloy is a binary alloy with the composition of about 50 at. % Ni and about 50 at. % Ti, which is one of the well-known shape-memory alloys. It has drawn tremendous interest in numerous fields, such as biomedical devices and implants [1], micro-actuators [2], robotics [3], and micro-electro-mechanical systems [4], because of the unique super-elasticity, shape memory effect, high strength, high corrosion resistance, high damping capacity, and excellent biocompatibility [5–9]. More and more researchers started to

* Corresponding author.
E-mail address: sandy.to@polyu.edu.hk (S. To).

https://doi.org/10.1016/j.jmrt.2023.05.214

study this smart material. Huang et al. [10] carried out the full atomic-level understanding of the NiTi alloy on its shape-memory effect based on the first-principles density functional study and found the shape memory was mainly stored at the microstructural level. Chen et al. [11] revealed the degeneration mechanisms of shape memory functions after the vacuum electron beam welding. Zhang et al. [12] investigated the effects of fabrication parameters of electron beam melting on the corrosion resistance of the NiTi alloy and observed that a superior corrosion resistance would be displayed when only some small pores were evenly distributed in this kind of alloy. For the forming methods of the NiTi alloy, forging and casting are commonly used. Yeom et al. [13] designed a hot forging process of this alloy according to deformation processing maps and obtained the optimum process design to fabricate a sound NiTi billet. But the traditional manufacturing processes face the problems of high production time, high production cost, high material waste, and low flexibility [14,15], which bring some inconvenience to the development and research of new materials.

Recently, additive manufacturing, also named three-dimensional (3D) printing, is gaining considerable attention due to its high efficiency, flexibility, economy, and environmental friendliness [16]. In the manufacturing process, a laser beam is employed to make metallic powder melt and solidify by using the contour information of a sliced computer-aided design (CAD) model [17]. After finishing one slice, the building platform moves downward until all slices have been finished. It can be found that in comparison with traditional manufacturing processes, the additive manufacturing does not need the use of dies and special tooling to produce metallic parts with complex geometry, which saves production time and reduces material waste [18,19]. Bagheri et al. [20] experimentally investigated and analyzed the cyclic deformation and the fatigue behavior of the additively manufactured (AMed) NiTi alloy at room temperature (~24 °C). Before the constant amplitude pulsating fatigue experiments, heat treating was used for all samples to decrease their plateau stress. Experimental results found the maximum stress level played a key influence on fatigue behaviors of NiTi alloy, and the microstructural defect like voids was the major reason for decreasing fatigue lives of the AMed NiTi alloy. In industrial applications, load-contact conditions significantly affect the pseudoelasticity behaviors, Zhang et al. [21] reported the influences of various load-contact conditions on pseudoelasticity behaviors of the AMed NiTi alloys and conducted indentation tests from the nanoscale to macroscale. Test results showed that pseudoelasticity behaviors at the nanoscale were the best regarding the smallest remnant depth ratios. Simultaneously, they also found that the enhancement in pseudoelasticity also caused the reduction in the Young's modulus and apparent hardness. In comparison with the macroscale components, micro-components, particularly the AMed micro-components, always exhibit different mechanical or functional properties. Xiong et al. [22] employed a micro laser powder bed fusion process to fabricate micro-NiTi parts, such as micro-stent and micro-lattice. Experimental results show that these micro-parts possessed superior mechanical properties. The compressive deformation reached 50% without mechanical failures and the shape recovery also could be up to >98% when heating.

However, the machining of the NiTi alloy is still a challenge due to its high ductility and severe strain-hardening [23], which easily leads to tool wear and burr formation [24]. Various machining processes were employed to cut NiTi alloys with high surface quality, high production efficiency, and low tool wear. Turning is a common machining process. For improving the machinability of the NiTi alloy, Zhao et al. [25] explored the influences of cooling conditions on the surface integrity, tool wear, and cutting force at different machining speeds. They found that cryogenic conditions achieved higher machinability when the cutting speed was 125 m/min. Milling is another machining process for removing workpiece materials and obtaining desired geometric structures. Weinert and Petzoldt [26] found that compared to dry milling, the application of the minimum quantity lubrication (MQL) could improve the workpiece quality and extend the tool life. Guo et al. [27] investigated the machinability and surface quality of the NiTi alloy using milling and electrical discharge machining. Experimental results found that the milling produced much better surface quality than the electrical discharge machining. At the same time, the tool wear mechanism during NiTi alloy milling was explored. The high dynamic strength led to the adhesion wear of the flank face, and the high heat caused the rake face wear. Although traditional turning and milling processes have been conducted to reduce tool wear and enhance machining quality, the machining of microstructure arrays on NiTi alloy surfaces is not studied exhaustively to date.

In this study, the systematic investigation of generating microstructure arrays on the AMed NiTi alloy surfaces is studied. The additive manufacturing of the NiTi alloy is introduced in Section 2. The ultraprecision micro-milling process is proposed to generate microstructure arrays on the AMed NiTi alloy surfaces. After the machining experiments, the micro-groove array and micro-pillar array are generated, and corresponding cutting forces, tool conditions, and chip morphologies are discussed to analyze the feasibility of generating microstructure arrays on AMed NiTi alloy surfaces in Section 3. Section 4 summarizes this study.

2. Materials and methods

2.1. *Additive manufacturing of NiTi alloy samples*

The selective laser melting is selected as a popular and well-established additive manufacturing process for fabricating NiTi alloy samples. The working principle of the selective laser melting is described graphically in Fig. 1(a). The NiTi powders are pre-placed on the build substrate to form a powder bed before additive manufacturing. The focus lenses are used to make the laser focus on the XY scanning mirror. Then the position of the focused laser is adjusted by the deflection of the XY scanning mirror to melt the NiTi powders [28,29]. After one layer is completed, the next powder layer is formed over the solidified part by the powder scraper until the sample is complete. The selective laser melting in this study was performed on a commercial laser additive manufacturing machine (SLM®125^{HL}, SLM Solutions Group AG, Germany), which mainly consisted of a continuous-wave fiber laser, a building chamber

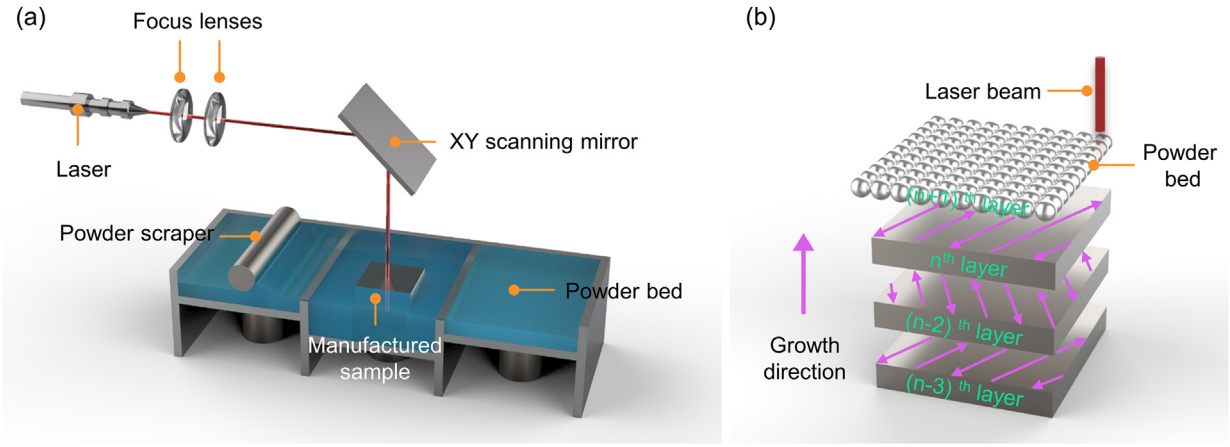

Fig. 1 – Schematic of (a) the selective laser melting and (b) scanning strategy.

with atmosphere control, an automatic powder scraper, a workbench, and a multi-axis motion system.

The scanning strategy of selective laser melting involves a zigzag path and 67° rotation between successive layers, as described in Fig. 1(b). After a series of trial runs, the optimized manufacturing parameters can be obtained: scanning speed 800 mm/s; layer thickness 40 μm; laser power 120 W; hatch spacing 100 μm. According to the scanning path and growth direction of each layer, the additively manufactured NiTi alloy samples with geometrical dimensions of 10 mm × 10 mm × 3 mm was obtained. Besides, a protective atmosphere was kept using ultrahigh purity grade argon gas to ensure an oxygen content below 100 ppm during additive manufacturing of NiTi alloy samples.

For raw materials of the selective laser melting, these NiTi powders with the chemical composition at %: 50.8 Ni and 49.2 Ti were used. A scanning electron microscope (SEM) (TM3000, Hitachi High-Technologies Corporation, Japan) was employed to characterize them. From SEM images, it can be found from Fig. 2(a) and (b) that the shape of NiTi powders is spherical. The particle size of NiTi powders in Fig. 2(a) was analyzed and measured by the ImageJ software. It is fitted by a Gaussian curve, as shown in Fig. 2(c). The average diameter of NiTi powders is about 40 μm. In addition, a small number of irregularly shaped particles and satellite powders were detected.

The phases formed in the AMed NiTi alloy sample were identified through an X-ray diffraction instrument (XRD, Shimadzu, XRD-7000, Japan) with Cu Kα (λ = 1.5406 Å) radiation at a scanning speed of 4°min^{-1}, ranging from 20° to 100° at 45 kV, and 200 mA. From Fig. 3, it can be found that the AMed NiTi alloy by the selective laser melting was mainly composed of an austenite phase at room temperature, Besides, there is no obvious secondary phase in the XRD spectrum.

2.2. *Machining experiments of microstructure arrays*

Ultraprecision micro-milling (UMM), as a micro/nano-machining process, can reach the nanometer-scale surface finish and high form accuracy. The machining experiments of as-built AMed NiTi alloy samples were conducted on an ultraprecision machining center (UVM-450C (V2), Toshiba Machine Co., Ltd., Japan) for generating microstructure arrays, as shown in Fig. 4(a). The machining center has two rotational axes (named A-axis and C-axis) and three linear axes (named

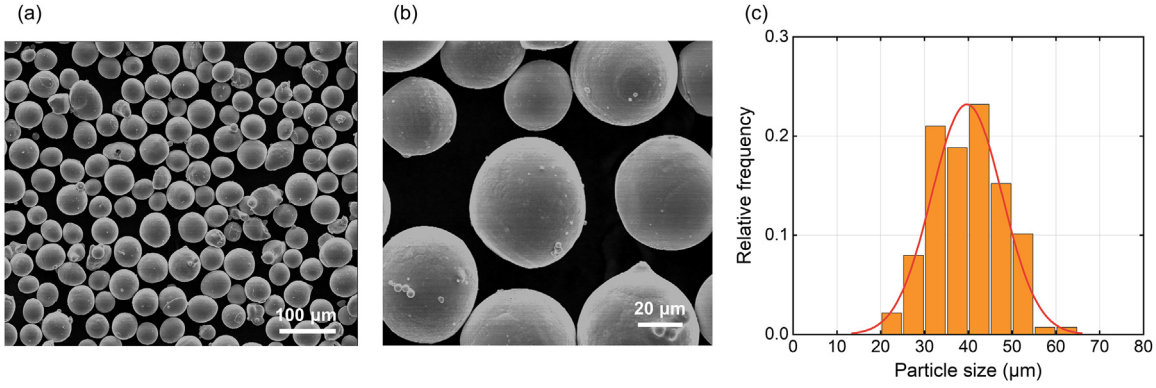

Fig. 2 – SEM images with (a) low magnification and (b) high magnification of NiTi powders; (c) particle size distribution of NiTi powders.

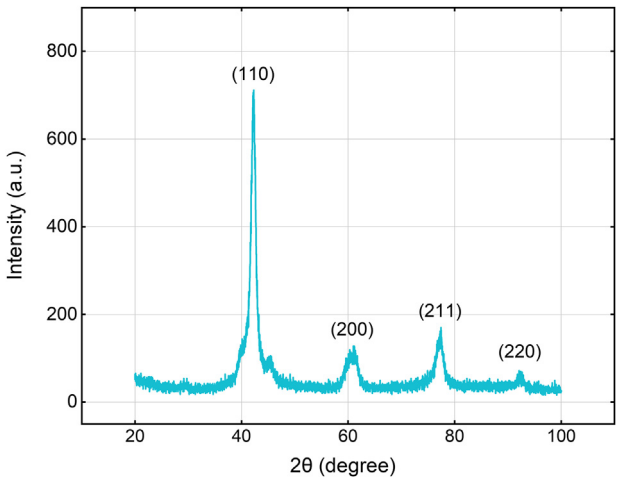

Fig. 3 – X-ray diffraction spectrum of the additively manufactured NiTi alloy sample.

X-axis, Y-axis, and Z-axis). And the programming resolution of three linear axes is 0.01 μm, which provides ultrahigh positioning accuracy for machining microstructure arrays. The non-repetitive run-out error of the A-axis (high-speed aerostatic bearing spindle) is 0.10 μm, which can realize high-quality machined surfaces. In the machining experiments, the workpiece (AMed NiTi alloy sample) with geometrical dimensions of 10 × 10 × 3 mm^3 was sticked to a fixture by the glue. And the fixture was installed on a dynamometer via the screws. The dynamometer was mounted on the C-axis of the machining center using a magnetic chuck, as presented in Fig. 4(b). During the machining of microstructure arrays, the milling tool was fixed to the A-axis to remove the workpiece material and generate the microstructure arrays. Two types of milling tools (2-flute end mill, NS TOOL Co.,Ltd, Japan) were used. Their models were MSE230 and MX230, respectively. The MSE230 had a diameter of 2 mm, which was used to flat the original workpiece surface and obtain a mirror surface with high surface quality, which included the rough machining and finish machining. The MX230 had a diameter of 0.2 mm and an available milling length of 0.4 mm, which was used to machine microstructure arrays on the AMed NiTi alloy surfaces. In all machining experiments, the MQL was employed via a nozzle to reduce machining heat. The detailed machining parameters of mirror surface machining and microstructure array machining are listed in Table 1.

Besides, a cutting force measurement system was established for obtaining the cutting forces during the machining of microstructure arrays. In this measurement system, a 3-component dynamometer (9256C1, Kistler Instrument Corp., Switzerland) with high sensitivity was used to generate the analogue signals based on the piezoelectric measurement principle, and then the analogue signals were amplified by a charge amplifier (5056, Multichannel Charge Amplifier, Kistler Instrument Corp., Switzerland). The amplified analogue signals were converted to digital signals by a multifunction I/O device (5697, Data Acquisition System, Kistler Instrument Corp., Switzerland). And the sampling rate was set at 20 kHz in this study, which was sufficient to capture the dynamic characteristics of the cutting forces during the machining experiments.

3. Results and discussion

3.1. *Characterization of microstructure arrays*

After the mirror surface machining, a mirror surface of the AMed NiTi alloy can be obtained, as shown in Fig. 5(a). A three-dimensional optical profiler with a sub-nanometer resolution (Nexview™, Zygo Corp., USA) was applied to measure the surface roughness and characterize the three-dimensional surface topography of this mirror surface. From the measurement result, the surface roughness (R_a) of the mirror surface is 14 nm, as presented in Fig. 5(b), which demonstrates the good machinability of the AMed NiTi alloy. It also preliminarily demonstrates the effectiveness of the proposed UMM process because it can achieve a lower surface roughness.

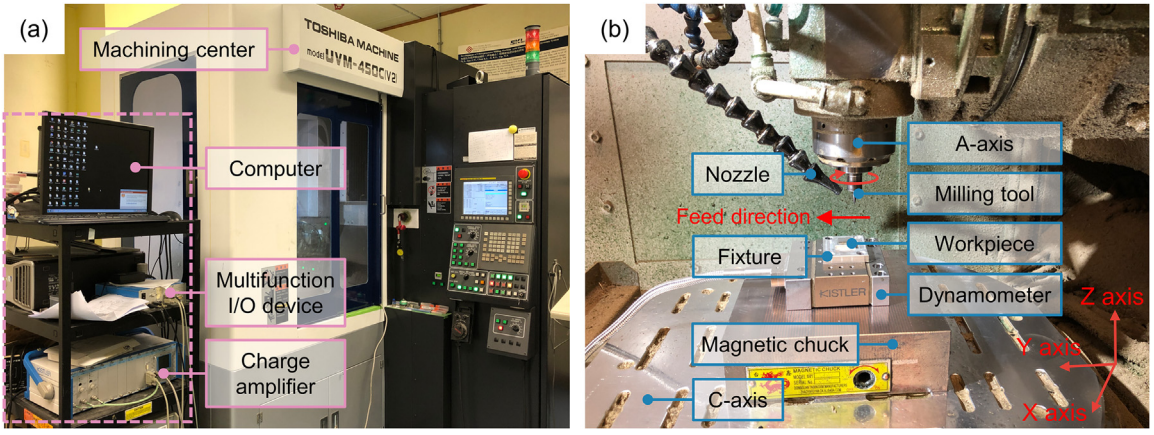

Fig. 4 – Photographs of the experimental setup. (a) Overview and (b) detailed view.

Table 1 – Machining parameters.

Mirror surface machining			Microstructure array machining		
Spindle speed (RPM)	Feed (mm/min)	Depth-of-cutting (mm)	Spindle speed (RPM)	Feed (mm/min)	Depth-of-cutting (mm)
60,000	300	Roughing machining: 0.03 Finishing machining: 0.01	60,000	300	0.01

Reasonable machining strategy can enhance the machining efficiency under the premise of ensuring machining quality [30,31] and it also can decrease or even avoid tool wear [32]. Fig. 6 illustrates the machining strategy of the UMM process for generating microstructure arrays on AMed NiTi alloy surfaces. Two types of microstructure arrays, named micro-groove array and micro-pillar array, are machined to demonstrate the feasibility of the proposed UMM process. To machine the micro-groove array, a flat end mill is selected as the milling tool to ensure that the micro-groove array has a rectangular profile. The flat end mill moves along the feed direction with an axial depth-of-cutting of 10 μm during machining. The cycle begins until the cumulative depth-of-cut reaches the design height of the micro-groove. Each cycle moves along the vertical direction of the feed, as shown in Fig. 6(a). For machining the micro-pillar array, the micro-groove array is firstly machined, and then the workpiece rotates 90° in an anticlockwise direction along the C-axis of the machine center. The next steps of the flat end mill keep the same as the machining of micro-groove arrays. Finally, a micro-pillar array is remained on the AMed NiTi alloy surface, as depicted in Fig. 6(d).

After the machining experiments, all AMed NiTi alloy samples were cleaned with an ultrasonic cleaner in ethanol for 10 min to wash off residual chips. The topographies of machined microstructure arrays were characterized by SEM. Fig. 7 shows the SEM images of the side view and top view of the micro-groove array and micro-pillar array. It can be seen that each micro-groove or micro-pillar has the same geometrical features (width, height, and geometrical form). To quantify the form accuracy of these microstructure arrays, the measurements about the width and height of the micro-groove and micro-pillar were taken three times to ensure reliability. For the micro-groove array, each micro-groove has the nearly same width (w) and height (h) in the whole machined area. The average values of the measured w and l of the micro-groove array are 198.1 μm and 378.3 μm. Taking the design dimensions (200 μm and 380.0 μm) as "true", the machining errors of the micro-groove array in terms of w and l are 0.95% and 0.45%. Similarly, the machining errors of the micro-pillar array in terms of width (w), length (l), and height (h) are 1.50%, 2.00%, and 1.05%, which again shows the high machining accuracy of the proposed UMM process in generating microstructure arrays on AMed NiTi alloy surfaces.

3.2. *Analysis of cutting forces*

Cutting force is an important parameter in the machining process [33]. The measurement of cutting forces during the machining of microstructure arrays can help to monitor and evaluate the proposed UMM process [34,35]. Fig. 8 quantitatively analyzes the cutting forces of one feed motion during the machining of the micro-groove array on the AMed NiTi alloy surface. F_x, F_y, and F_z denote the cutting forces in the vertical direction of feed, feed direction, and depth-of-cutting direction, as shown in Fig. 6. From Fig. 8(a), (b), and (c), the average peak-to-valley values of F_x, F_y, and F_z can be obtained and they are 1.01 N, 0.91 N, and 0.44 N, respectively. The

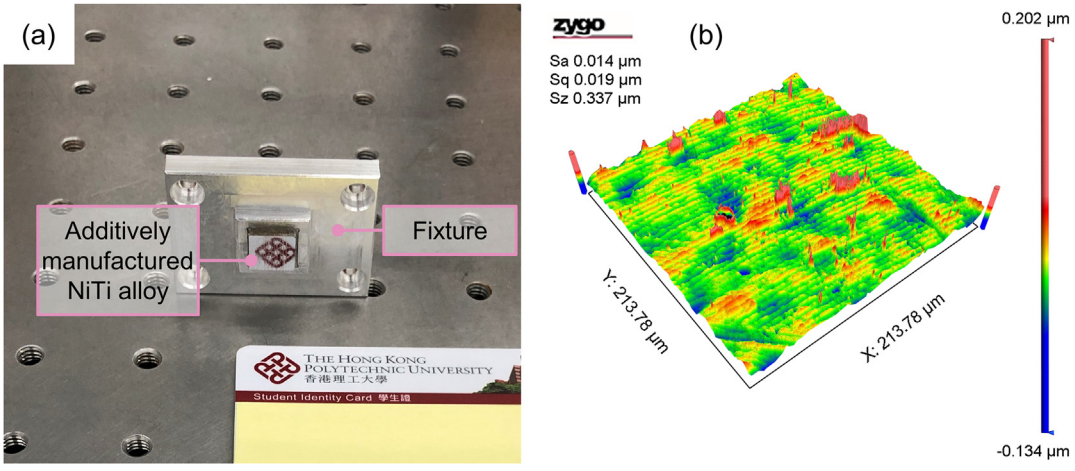

Fig. 5 – (a) Photograph and (b) surface roughness of an additively manufactured NiTi alloy sample after mirror surface machining.

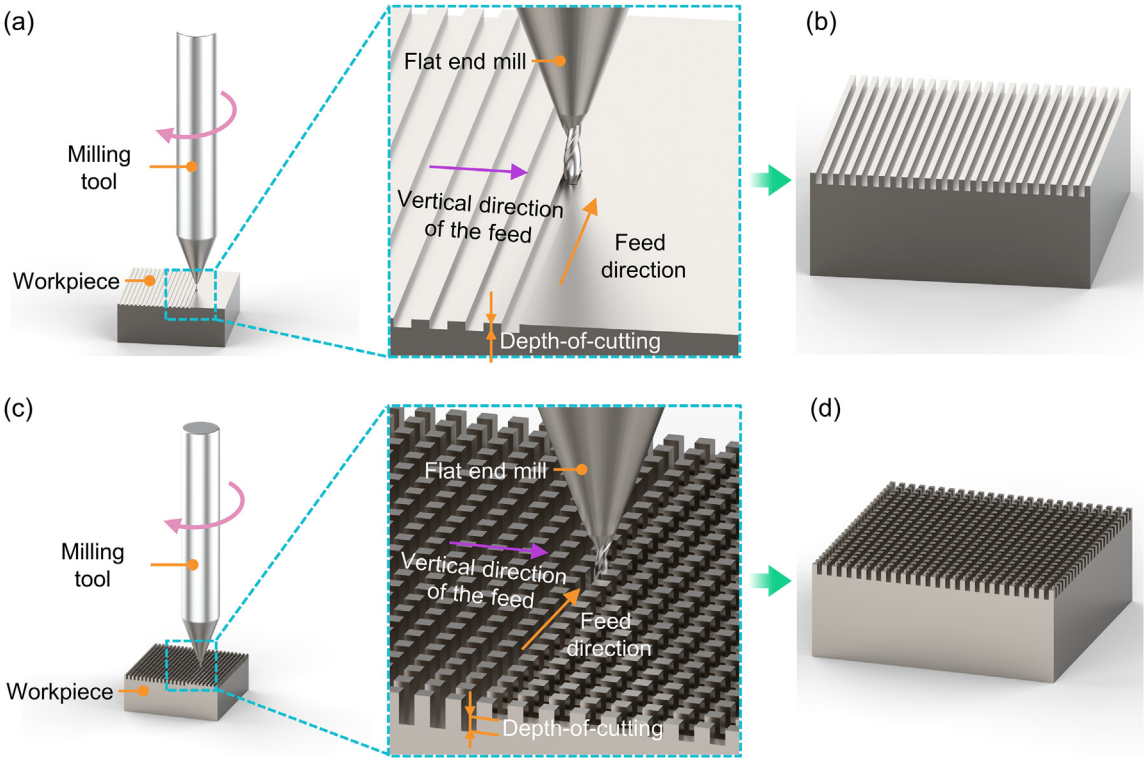

Fig. 6 – Schematic of the ultraprecision micro-milling strategy of microstructure arrays.

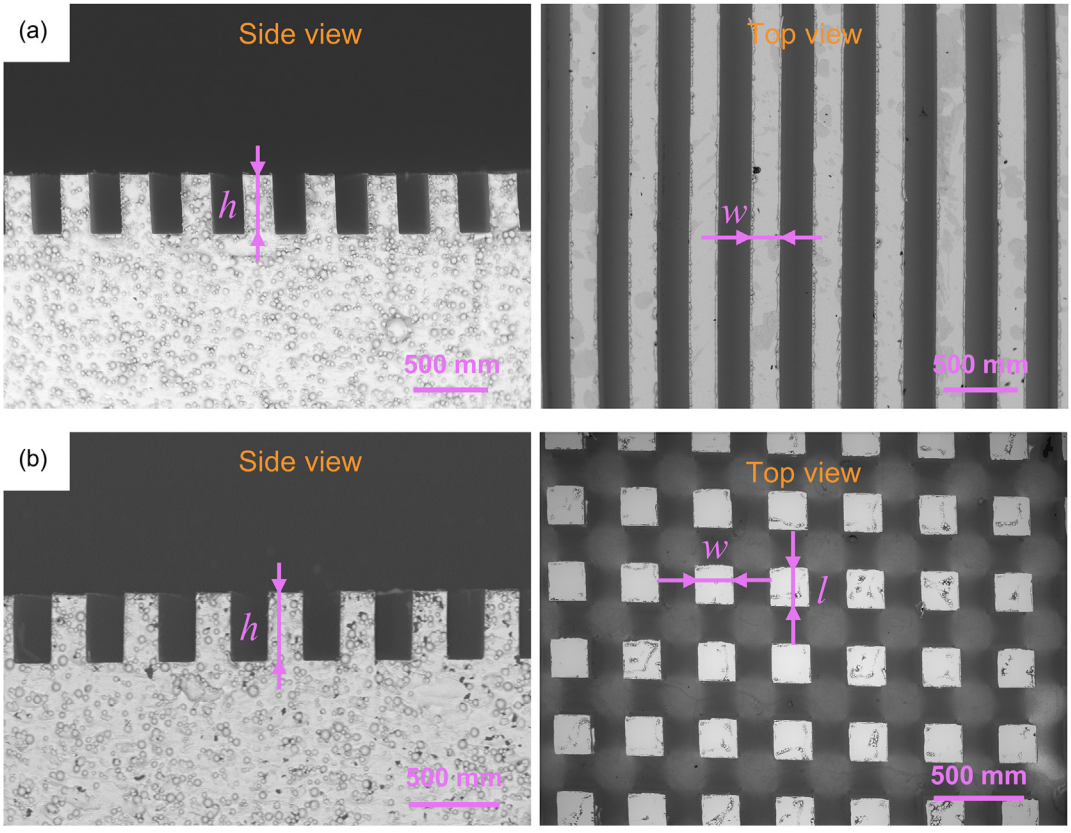

Fig. 7 – SEM images of (a) the micro-groove array and (b) micro-pillar array.

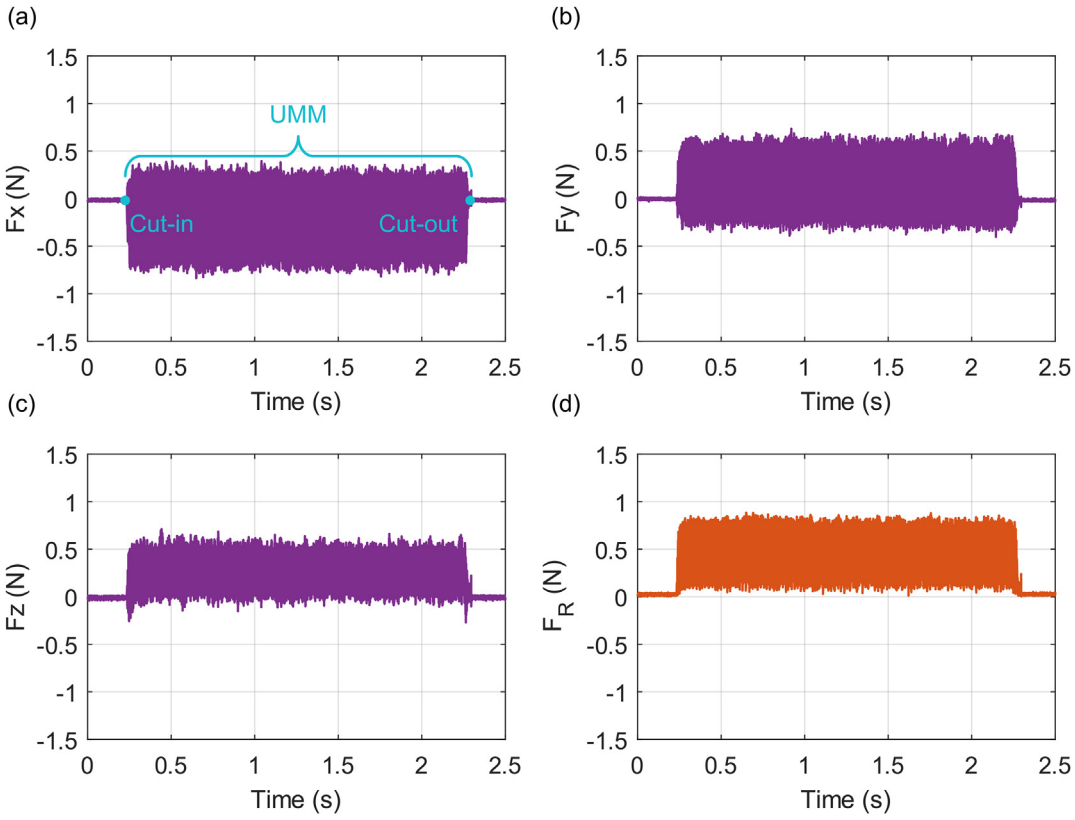

Fig. 8 – Measured cutting forces during the machining of the microstructure array on additively manufactured NiTi alloy surfaces.

average value of cutting forces in the vertical direction of feed and feed direction is around two times larger than that of cutting forces in the depth-of-cutting direction. It is because more workpiece materials are removed along the feed-related motions during machining. Removing more workpiece material needs larger cutting forces.

The resultant cutting forces (F_R) can be calculated. And F_R is the square root of the sum of squares of the F_x, F_y, and F_z. They are plotted in Fig. 8(d). It is clearly observed that the maximum of resultant cutting forces is less than 1 N. The low cutting forces demonstrate the proposed UMM process can be applied in generating microstructure arrays on AMed NiTi alloy surfaces. In addition, it also further demonstrates that the AMed NiTi alloy has good machinability.

3.3. *Observation of tool wear condition*

In the ultraprecision machining field, tool wear easily occurs since the diameter of the milling tool is relatively small, generally less than 500 μm. So, the tool conditions after machining need to be observed. Fig. 9 presents the SEM images of the milling tools that were used in this study. There is a little material adhesion on the end flank face (along the end cutting edge) after machining the mirror surface (about 11 min), machining the micro-groove array (about 51 min), and machining the micro-pillar array (about 102 min), as presented in Fig. 9(a), (b), and (c). But in comparison with the new cutting tool shown in Fig. 9(d), no noticeable tool wear, such as micro-chipping, crater wear, and flank wear [36], was found by observing the rake face, cutting edge, and flank face. Because the MQL technique was applied in this study, and the high-pressure oil mist in the MQL technique can serve as the lubrication and antifriction [37], which benefits to reduce tool wear and increase tool life. It also indicates that the proposed UMM process is very appropriate for generating microstructure arrays on AMed NiTi alloy surfaces.

3.4. *Investigation of chip morphologies*

Machining is a material failure process [38]. When the milling tool increasingly enters into the workpiece, the workpiece material will undergo plastic deformation and then chips will be formed [39]. Therefore, apart from the study of cutting forces and tool conditions, the investigation of the chip morphologies is also needed, which will help to understand the material removal mechanism for industrial-scale machining of the AMed NiTi alloy. Chips were collected randomly for each machining in this study and then were observed by the SEM. The chips morphologies under different machining conditions (rough machining of the mirror surface, finish machining of the mirror surface, micro-groove array machining, and micro-pillar array machining) are shown in Fig. 10. First, the chip morphology in the roughing machining of the mirror surface is considerably different from the

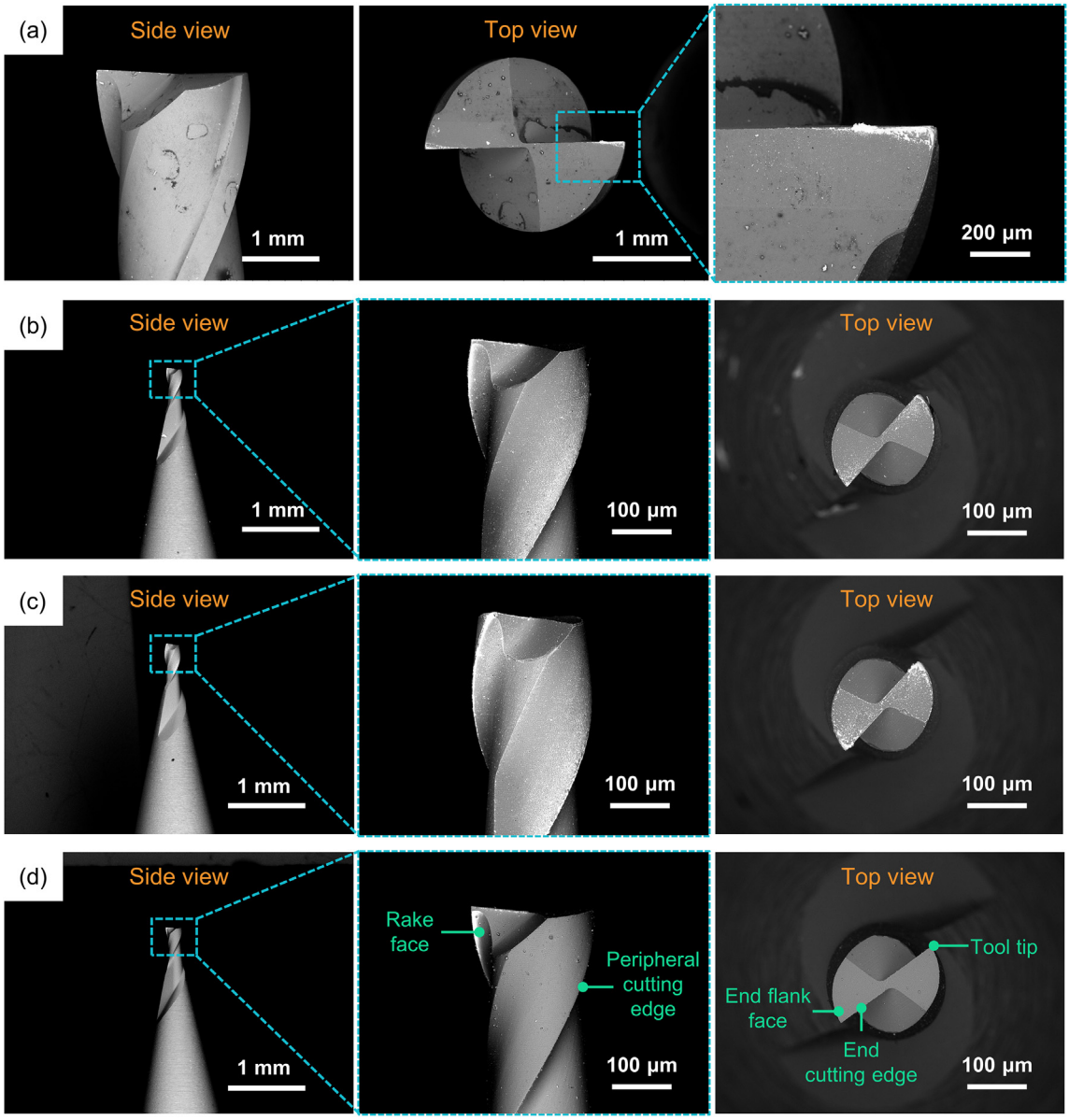

Fig. 9 – SEM images of the milling tools after machining experiments. (a) milling tool after machining the mirror surface, (b) milling tool after machining the micro-groove array, (c) milling tool after machining the micro-pillar array, and (d) new milling tool.

finishing machining of the mirror surface, the micro-groove array machining, and the micro-pillar array machining. The segmented chips in roughing machining of the mirror surface were formed, as shown in Fig. 10(a), while the long ribbon-shaped chips were formed in other machining, as presented in Fig. 10(b)–(d). The huge crack in segmented chips indicates the existence of a plastic fracture in rough machining of the mirror surface [40]. The only difference in machining parameters was the depth-of-cutting. Therefore, the large depth-of-cutting (30 μm) in rough machining of the mirror surface leads to this phenomenon [41]. Second, the chip morphologies in finishing machining of the mirror surface, micro-groove array machining, and micro-pillar array machining look the same, as shown in Fig. 10(b)–(d). The lamella structures were formed on the free surface of long and continuous chips, which is similar to most metallic materials. The fine lamella structures further indicate good ductility and machinability of the AMed NiTi alloy.

3.5. *Surface wettability of microstructure arrays*

Microstructure arrays often make the engineering material possess surprising surface functions, which can be found in our previous study [42,43]. Surface wettability is an indicator to depict these surface functions, which can be quantitatively evaluated using the contact angle between the droplet and

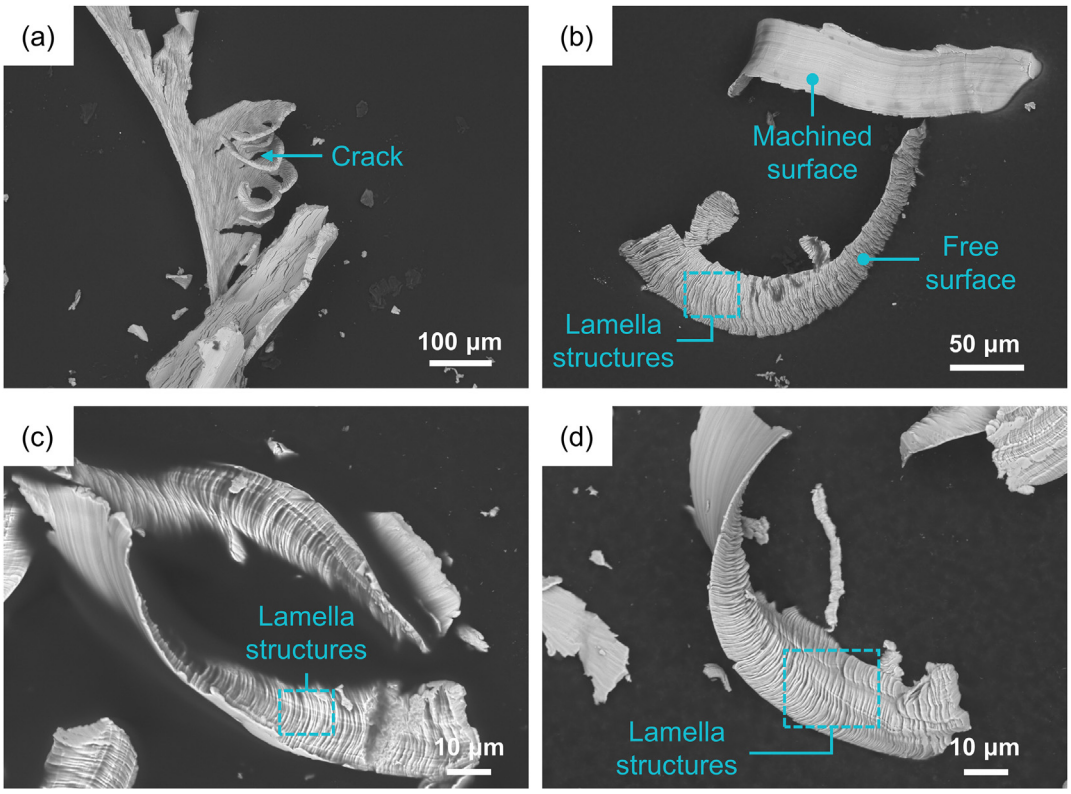

Fig. 10 – SEM images of chip morphologies under different machining conditions. (a) Rough machining of the mirror surface, (b) finish machining of the mirror surface, (c) micro-groove array machining, and (d) micro-pillar array machining.

material surface [44,45]. If the contact angle is lower than 90°, this indicates that the material surface processes a hydrophilicity property. If the contact angle is larger than 90°, this indicates that the material surface processes a hydrophobicity property [46,47]. Fig. 11 shows the experimental setup of measuring contact angle in this study. A goniometer (model 100SB, Sindatek Instruments Co., Ltd., China) was applied to measure the contact angle, which was composed of a homogeneous LED light source, a computer-controlled syringe pump, a sample stage, and a high-resolution camera. A deionized water droplet was used to measure the contact angle, and its volume (5 μl) was precisely controlled by the computer-controlled syringe pump. The contact angle in a steady state of the deionized water droplet in a room temperature was calculated by a commercial software named DropMeter. Each measurement was conducted five times and the average value was recorded along with a standard deviation to ensure reliability.

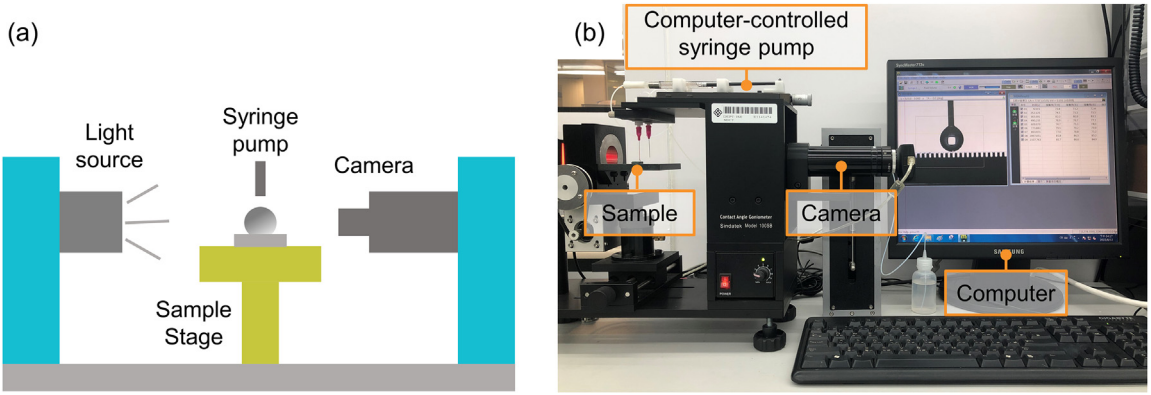

Fig. 11 – (a) Schematic and (b) photograph of the experimental setup of measuring contact angle.

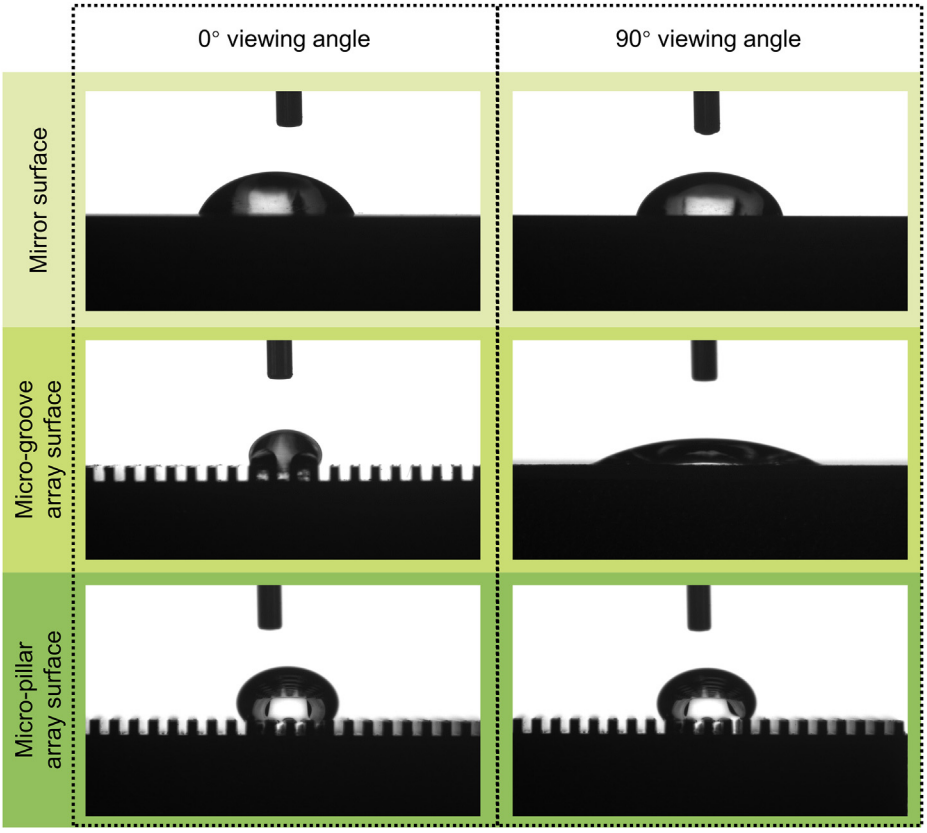

Fig. 12 – Different wetting states of the water droplets.

Fig. 12 shows the wetting status of the water droplets on different microstructure array surfaces. The 0° viewing angle denotes the viewing direction (also measurement direction) is parallel with the micro-groove array direction. Similarly, the 90° viewing angle denotes the viewing direction is perpendicular to the micro-groove array direction. The static contact angles were measured along these two directions to quantitatively analyze the surface wettability of microstructure arrays, as shown in Fig. 13. It is confirmed that the surface wettability has been obviously modified using the UMM process. The contact angles of the mirror surface at the 0° viewing angle and 90° viewing angle are

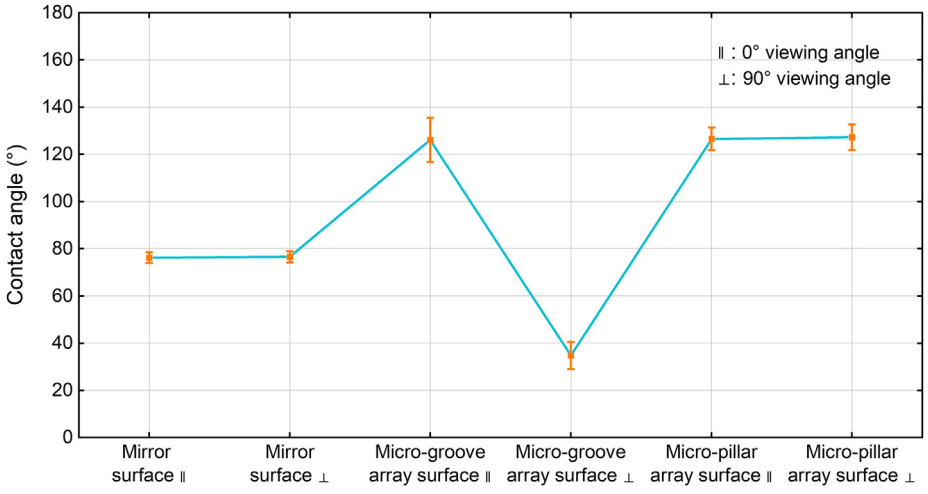

Fig. 13 – Measured contact angles on different microstructure array surfaces.

76.18 ± 2.27° and 76.58 ± 2.38°. They keep almost the same. However, the contact angles of the micro-groove array surface show a noticeable difference at different viewing angles. The contact angle at 0° viewing angle is 126.05 ± 9.39° while it at 90° viewing angle is 34.7 ± 5.74°. The micro-groove array makes the AMed NiTi alloy sample anisotropy. The water droplet on the micro-groove array rests with a strip instead of a sphere due to its movement and spreading along the micro-groove array [48,49]. The contact angle of the micro-pillar array surface at the 0° viewing angle and 90° viewing angle also keeps the same, but the average value of the contact angle is around 127.0°, which shows the micro-pillar array surface possesses a hydrophobic property. Compared with the mirror surface, the contact angle has increased by 66.27%. It again demonstrates the surface property of the AMed NiTi alloy can be modified by the proposed UMM process, which can be applied to reduction of condensate retention, self-cleaning, and anti-foul of the AMed NiTi alloy in the future.

4. Conclusions

In this work, NiTi alloy samples were additively manufactured by selective laser melting. The ultraprecision micro-milling (UMM) process was proposed to generate the microstructure arrays on the additively manufactured (AMed) NiTi alloy surfaces. The corresponding microstructure array topographies, cutting forces, tool conditions, chip morphologies, and surface wettability were comprehensively studied. The main findings are summarized as follows.

(1) The microstructure arrays (micro-groove array and micro-pillar array) were generated on the AMed NiTi alloy surfaces by the proposed UMM process. In comparison with the design dimensions, the average machining errors for the micro-groove array and micro-pillar array are 0.7% and 1.51%, which demonstrates the high machining accuracy of the proposed UMM process.
(2) The cutting forces, tool conditions, and chip morphologies, as important indicators of machining features, were quantitatively analyzed after machining experiments. The lower cutting forces (the peak-to-valley value is less than 1 N), no obvious tool wear, and ribbon-shaped chips verify the feasibility of the proposed UMM process for generating microstructure arrays.
(3) The surface wettability of microstructure arrays was explored by measuring contact angles. The experimental results show that the droplet contact angle of the micro-pillar array surface is increased by 66.27% compared to the mirror surface. The original surface (hydrophilic surface) is converted into the hydrophobic surface, which shows that the proposed UMM process has the ability to tailor the surface property of the AMed NiTi alloy.

This study provides a facial and flexible ultraprecision machining process for generating microstructure arrays on additively manufactured NiTi alloy surfaces, which helps establish a scientific and systematic understanding of the machinability of additively manufactured materials. Besides, this study also provides an environmentally friendly method, using mechanical machining rather than chemical coatings, for tailoring the surface wettability, which can expand the application ranges of additively manufactured materials to self-cleaning, anti-foul, and drag reduction in the future.

Credit authorship contribution statement

Hanheng Du: Conceptualization, Methodology, Software, Validation, Formal analysis, Investigation, Data curation, Writing - Original Draft, Writing - Review & Editing, Visualization. **Chenliang Wu:** Investigation, Formal analysis. **Denghui Li:** Investigation. **Wai Sze Yip:** Supervision. **Zuankai Wang:** Supervision. **Suet To:** Resources, Supervision, Project administration, Funding acquisition, Writing - Review & Editing.

Data availability

Data will be made available on request.

Declaration of competing interest

The authors declare that they have no known competing financial interests or personal relationships that could have appeared to influence the work reported in this paper.

Acknowledgments

This work was funded by the Research Grants Council of the Hong Kong Special Administrative Region, China (Project No.: PolyU 15221322), the National Natural Science Foundation of China (Project No.: U19A20104), the Shenzhen Science and Technology Program (Project No.: JCYJ20210324131214039), and State Key Laboratory of Ultra-precision Machining Technology.

REFERENCES

[1] Chan W-S, Gulati K, Peters OA. Advancing Nitinol: from heat treatment to surface functionalization for nickel–titanium (NiTi) instruments in endodontics. Bioact Mater 2023;22:91–111. https://doi.org/10.1016/J.BIOACTMAT.2022.09.008.
[2] Seok S, Onal CD, Cho KJ, Wood RJ, Rus D, Kim S. Meshworm: a peristaltic soft robot with antagonistic nickel titanium coil actuators. IEEE/ASME Trans Mechatronics 2013;18:1485–97. https://doi.org/10.1109/TMECH.2012.2204070.
[3] Wang W, Ahn SH. Shape memory alloy-based soft gripper with variable stiffness for compliant and effective grasping. Soft Robot 2017;4:379–89. https://doi.org/10.1089/soro.2016.0081.
[4] Clare AT, Chalker PR, Davies S, Sutcliffe CJ, Tsopanos S. Selective laser melting of high aspect ratio 3D nickel-titanium structures two way trained for MEMS applications.

Int J Mech Mater Des 2008;4:181–7. https://doi.org/10.1007/s10999-007-9032-4.
[5] Mohd Jani J, Leary M, Subic A, Gibson MA. A review of shape memory alloy research, applications and opportunities. Mater Des 2014;56:1078–113. https://doi.org/10.1016/J.MATDES.2013.11.084.
[6] Gómez-Cortés JF, Nó ML, López-Ferrenõ I, Hernández-Saz J, Molina SI, Chuvilin A, et al. Size effect and scaling power-law for superelasticity in shape-memory alloys at the nanoscale. Nat Nanotechnol 2017;12:790–6. https://doi.org/10.1038/nnano.2017.91.
[7] Hua P, Xia M, Onuki Y, Sun Q. Nanocomposite NiTi shape memory alloy with high strength and fatigue resistance. Nat Nanotechnol 2021;16:409–13. https://doi.org/10.1038/s41565-020-00837-5.
[8] Li X, Chen X, Zhang C, Luo J. Preparation of self-lubricating NiTi alloy and its self-adaptive behavior. Tribol Int 2019;130:43–51. https://doi.org/10.1016/j.triboint.2018.09.002.
[9] Coon ME, Stephan SB, Gupta V, Kealey CP, Stephan MT. Nitinol thin films functionalized with CAR-T cells for the treatment of solid tumours. Nat Biomed Eng 2020;4. https://doi.org/10.1038/s41551-019-0486-0.
[10] Huang X, Ackland GJ, Rabe KM. Crystal structures and shape-memory behaviour of NiTi. Nat Mater 2003;2:307–11. https://doi.org/10.1038/nmat884.
[11] Chen G, Liu J, Dong Z, Li Y, Zhao Y, Zhang B, et al. Understanding mechanisms of shape memory function deterioration for nitinol alloy during non-equilibrium solidification by electron beam. J Adv Res 2021;33:99–108. https://doi.org/10.1016/J.JARE.2021.02.007.
[12] Zhang L, Ren D, Ji H, Ma A, Daniel EF, Li S, et al. Study on the corrosion behavior of NiTi shape memory alloys fabricated by electron beam melting. Npj Mater Degrad 2022;6:1–8. https://doi.org/10.1038/s41529-022-00289-3.
[13] Yeom JT, Kim JH, Hong JK, Kim SW, Park CH, Nam TH, et al. Hot forging design of as-cast NiTi shape memory alloy. Mater Res Bull 2014;58:234–8. https://doi.org/10.1016/J.MATERRESBULL.2014.04.049.
[14] Achillas C, Tzetzis D, Raimondo MO. Alternative production strategies based on the comparison of additive and traditional manufacturing technologies. Int J Prod Res 2017;55:3497–509. https://doi.org/10.1080/00207543.2017.1282645.
[15] Attaran M. The rise of 3-D printing: the advantages of additive manufacturing over traditional manufacturing. Bus Horiz 2017;60:677–88. https://doi.org/10.1016/J.BUSHOR.2017.05.011.
[16] Liu F, Xie H, He W. Multi-field coupling fatigue behavior of laser additively manufactured metallic materials: a review. J Mater Res Technol 2023;22:2819–43. https://doi.org/10.1016/j.jmrt.2022.12.112.
[17] Nguyen HD, Pramanik A, Basak AK, Dong Y, Prakash C, Debnath S, et al. A critical review on additive manufacturing of Ti-6Al-4V alloy: microstructure and mechanical properties. J Mater Res Technol 2022;18:4641–61. https://doi.org/10.1016/j.jmrt.2022.04.055.
[18] Shah N, D MJ, R MR, Phanikumar G. Microstructure prediction of eutectic high entropy alloy using physical and computer simulation for additive manufacturing condition. J Alloys Compd 2022;929:167268. https://doi.org/10.1016/j.jallcom.2022.167268.
[19] Chen C, Ling C, Shao Y, Yang Y, Wang D, Shuai C. Quasicrystal-strengthened biomedical magnesium alloy fabricated by laser additive manufacturing. J Alloys Compd 2023;947:169555. https://doi.org/10.1016/j.jallcom.2023.169555.
[20] Bagheri A, Mahtabi MJ, Shamsaei N. Fatigue behavior and cyclic deformation of additive manufactured NiTi. J Mater Process Technol 2018;252:440–53. https://doi.org/10.1016/J.JMATPROTEC.2017.10.006.
[21] Zhang D, Li Y, Cong W. Multi-scale pseudoelasticity of NiTi alloys fabricated by laser additive manufacturing. Mater Sci Eng, A 2021;821:141600. https://doi.org/10.1016/J.MSEA.2021.141600.
[22] Xiong Z, Li H, Yang H, Yang Y, Liu Y, Cui L, et al. Micro laser powder bed fusion of NiTi alloys with superior mechanical property and shape recovery function. Addit Manuf 2022;57:102960. https://doi.org/10.1016/J.ADDMA.2022.102960.
[23] Elahinia MH, Hashemi M, Tabesh M, Bhaduri SB. Manufacturing and processing of NiTi implants: a review. Prog Mater Sci 2012;57:911–46. https://doi.org/10.1016/J.PMATSCI.2011.11.001.
[24] Weinert K, Petzoldt V, Kötter D. Turning and drilling of NiTi shape memory alloys. CIRP Ann - Manuf Technol 2004;53. https://doi.org/10.1016/S0007-8506(07)60646-5.
[25] Zhao Y, Guo K, Li J, Sun J. Investigation on machinability of NiTi shape memory alloys under different cooling conditions. Int J Adv Manuf Technol 2021;116:1913–23. https://doi.org/10.1007/s00170-021-07563-9.
[26] Weinert K, Petzoldt V. Machining NiTi micro-parts by micro-milling. Mater Sci Eng, A 2008;481:672–5. https://doi.org/10.1016/J.MSEA.2006.10.220. 482.
[27] Guo Y, Klink A, Fu C, Snyder J. Machinability and surface integrity of Nitinol shape memory alloy. CIRP Ann 2013;62:83–6. https://doi.org/10.1016/J.CIRP.2013.03.004.
[28] Chen Q, Guillemot G, Gandin CA, Bellet M. Three-dimensional finite element thermomechanical modeling of additive manufacturing by selective laser melting for ceramic materials. Addit Manuf 2017;16:124–37. https://doi.org/10.1016/J.ADDMA.2017.02.005.
[29] Jiang Q, Zhang P, Yu Z, Shi H, Wu D, Yan H, et al. A review on additive manufacturing of pure copper. Coatings 2021;11. https://doi.org/10.3390/coatings11060740.
[30] Danish M, Aslantas K, Hascelik A, Rubaiee S, Gupta MK, Yildirim MB, et al. An experimental investigations on effects of cooling/lubrication conditions in micro milling of additively manufactured Inconel 718. Tribol Int 2022;173:107620. https://doi.org/10.1016/j.triboint.2022.107620.
[31] Cao H, Liu L, Wu B, Gao Y, Qu D. Process optimization of high-speed dry milling UD-CF/PEEK laminates using GA-BP neural network. Compos B Eng 2021:221. https://doi.org/10.1016/j.compositesb.2021.109034.
[32] De Aguiar MM, Diniz AE, Pederiva R. Correlating surface roughness, tool wear and tool vibration in the milling process of hardened steel using long slender tools. Int J Mach Tool Manufact 2013;68:1–10. https://doi.org/10.1016/j.ijmachtools.2013.01.002.
[33] Behera BC, Ghosh S, Rao PV. Modeling of cutting force in MQL machining environment considering chip tool contact friction. Tribol Int 2018;117:283–95. https://doi.org/10.1016/j.triboint.2017.09.015.
[34] Zhang X, Yu T, Wang W. Prediction of cutting forces and instantaneous tool deflection in micro end milling by considering tool run-out. Int J Mech Sci 2018;136. https://doi.org/10.1016/j.ijmecsci.2017.12.019.
[35] Pérez-Ruiz JD, de Lacalle LNL, Urbikain G, Pereira O, Martínez S, Bris J. On the relationship between cutting forces and anisotropy features in the milling of LPBF Inconel 718 for near net shape parts. Int J Mach Tool Manufact

2021;170:103801. https://doi.org/10.1016/j.ijmachtools.2021.103801.
[36] Race A, Zwierzak I, Secker J, Walsh J, Carrell J, Slatter T, et al. Environmentally sustainable cooling strategies in milling of SA516: effects on surface integrity of dry, flood and MQL machining. J Clean Prod 2021;288:125580. https://doi.org/10.1016/J.JCLEPRO.2020.125580.
[37] Giasin K, Ayvar-Soberanis S, Hodzic A. The effects of minimum quantity lubrication and cryogenic liquid nitrogen cooling on drilled hole quality in GLARE fibre metal laminates. Mater Des 2016;89:996–1006. https://doi.org/10.1016/j.matdes.2015.10.049.
[38] Palaniappan K, Sundararaman M, Murthy H, Jeyaraam R, Rao BC. Influence of workpiece texture and strain hardening on chip formation during machining of Ti–6Al–4V alloy. Int J Mach Tool Manufact 2022;173:103849. https://doi.org/10.1016/J.IJMACHTOOLS.2021.103849.
[39] Wang Y, Zou B, Wang J, Wu Y, Huang C. Effect of the progressive tool wear on surface topography and chip formation in micro-milling of Ti–6Al–4V using Ti(C7N3)-based cermet micro-mill. Tribol Int 2020;141:105900. https://doi.org/10.1016/J.TRIBOINT.2019.105900.
[40] Pacella M. A new low-feed chip breaking tool and its effect on chip morphology. Int J Adv Manuf Technol 2019;104:1145–57. https://doi.org/10.1007/s00170-019-03961-2.
[41] Niu Z, Jiao F, Cheng K. An innovative investigation on chip formation mechanisms in micro-milling using natural diamond and tungsten carbide tools. J Manuf Process 2018;31:382–94. https://doi.org/10.1016/J.JMAPRO.2017.11.023.
[42] Feng S, Zhu P, Zheng H, Zhan H, Chen C, Li J, et al. Three-dimensional capillary ratchet-induced liquid directional steering. Science 2021;373:1344–8. https://doi.org/10.1126/science.abg7552. 80-.
[43] Jiang M, Wang Y, Liu F, Du H, Li Y, Zhang H, et al. Inhibiting the Leidenfrost effect above 1,000 °C for sustained thermal cooling. Nature 2022;601:568–72. https://doi.org/10.1038/s41586-021-04307-3.
[44] Meiron TS, Marmur A, Saguy IS. Contact angle measurement on rough surfaces. J Colloid Interface Sci 2004;274:637–44. https://doi.org/10.1016/J.JCIS.2004.02.036.
[45] Shams H, Basit K, Khan MA, Mansoor A, Saleem S. Scalable wear resistant 3D printed slippery liquid infused porous surfaces (SLIPS). Addit Manuf 2021;48:102379. https://doi.org/10.1016/J.ADDMA.2021.102379.
[46] Commentary G. Definitions for hydrophilicity, hydrophobicity, and superhydrophobicity: getting the basics right. J Phys Chem Lett 2014;5:686–8.
[47] Ding Y, Jia L, Peng Q, Guo J. Critical sliding angle of water droplet on parallel hydrophobic grooved surface. Colloids Surfaces A Physicochem Eng Asp 2020;585:124083. https://doi.org/10.1016/J.COLSURFA.2019.124083.
[48] Li W, Fang G, Li Y, Qiao G. Anisotropic wetting behavior arising from superhydrophobic surfaces: parallel grooved structure. J Phys Chem B 2008;112:7234–43. https://doi.org/10.1021/jp712019y.
[49] Shi Z, Liu Z, Song H, Zhang X. Prediction of contact angle for hydrophobic surface fabricated with micro-machining based on minimum Gibbs free energy. Appl Surf Sci 2016;364:597–603. https://doi.org/10.1016/J.APSUSC.2015.12.199.